Journal of Clinical and Translational Hepatology **2023**
DOI: 10.14218/JCTH.2022.00110

Original Article

Therapeutic Effect of Prolyl Endopeptidase Inhibitor in High-fat Diet-induced Metabolic Dysfunction-associated Fatty Liver Disease

Jian-Bin Zhang[1,2#], Meng-Ting Li[1,3#], Shuang-Zhe Lin[1], Yu-Qing Cheng[1], Jian-Gao Fan[1*] and Yuan-Wen Chen[2,4*]

[1]Department of Gastroenterology, Xinhua Hospital, Shanghai Jiaotong University School of Medicine, Shanghai, China; [2]Department of Gastroenterology, Huadong Hospital, Fudan University, Shanghai, China; [3]Department of Gastroenterology, The Affiliated People's Hospital of Ningbo University, Ningbo, Zhejiang, China; [4]Department of Geriatrics, Huadong Hospital, Fudan University, Shanghai, China

Received: 15 November 2022 | **Revised:** 13 February 2023 | **Accepted:** 27 February 2023 | **Published online:** 19 April 2023

Abstract

Background and Aims: Prolyl endopeptidase (PREP) is a serine endopeptidase that participates in many pathological processes including inflammation, oxidative stress, and autophagy. Our previous studies found that PREP knockout exhibited multiple benefits in high-fat diet (HFD) or methionine choline-deficient diet-induced metabolic dysfunction-associated fatty liver disease (MAFLD). However, cumulative studies have suggested that PREP performs complex functions during disease development. Therefore, further understanding the role of PREP in MAFLD development is the foundation of PREP intervention. ***Methods:*** In this study, an HFD-induced MAFLD model at different time points (4, 8, 12, and 16 weeks) was used to explore dynamic changes in the PREP proline-glycine-proline (PGP)/N-acetyl-seryl-aspartyl-lysyl-proline (AcSDKP) system. To explore its potential value in MAFLD treatment, saline, or the PREP inhibitor, KYP-2047, was administered to HFD-induced MAFLD mice from the 10th to 16th weeks. ***Results:*** PREP activity and expression were increased in HFD-mice compared with control mice from the 12th week onwards, and increased PREP mainly resulted in the activation of the matrix metalloproteinase 8/9 (MMP8/9)-PREP-PGP axis rather than the thymosin β4-meprin α/PREP-AcSDKP axis. In addition, KYP-2047 reduced HFD-induced liver injury and oxidative stress, improved lipid metabolism through the suppression of lipogenic genes and the induction of β-oxidation-related genes, and attenuated hepatic inflammation by decreasing MMP8/9 and PGP. Moreover, KYP2047 restored HFD-induced impaired autophagy and this was verified in HepG2 cells. ***Conclusions:*** These findings suggest that increased PREP activity/expression during MAFLD development might be a key factor in the transition from simple steatosis to steatohepatitis, and KYP-2047 might possess therapeutic potential for MAFLD treatment.

Citation of this article: Zhang JB, Li MT, Lin SZ, Cheng YQ, Fan JG, Chen YW. Therapeutic Effect of Prolyl Endopeptidase Inhibitor in High-fat Diet-induced Metabolic Dysfunction-associated Fatty Liver Disease. J Clin Transl Hepatol 2023. doi: 10.14218/JCTH.2022.00110.

Keywords: Metabolic dysfunction-associated fatty liver disease; Prolyl endopeptidase; KYP-2047; Proline-glycine-proline; N-acetyl-seryl-aspartyl-lysyl-proline.

Abbreviations: α-SMA, α-smooth muscle actin; ACACA, acetyl CoA carboxylase-alpha; ACOX1, acyl coenzyme A oxidase1; AcSDKP, N-acetyl-seryl-aspartyl-lysyl-proline; ALP, alkaline phosphatase; ALT, alanine aminotransferase; AST, aspartate aminotransferase; BSA, bovine serum albumin; CAT, catalase; CCl4, carbon tetrachloride; COL1A1, collagen type I alpha 1 chain; COL3A1, collagen type III alpha 1 chain; CYP7A1, cholesterol 7-alpha hydroxylase; DMSO, dimethylsulfoxide; FBG, fasting blood glucose; GAPDH, Glyceraldehyde 3-phosphate dehydrogenase; HE, Hematoxylin and eosin; HFD, high-fat diet; HOMA-IR, homeostasis model assessment of insulin resistance; IL-1β, interleukin-1β; LCN2, lipocalin-2; LDH, lactate dehydrogenase; LDL-C, low-density lipoprotein cholesterol; MAFLD, metabolic Dysfunction-Associated Fatty Liver Disease; MCD, methionine-choline-deficient; MMP8/9, matrix metalloproteinases 8/9; MPO, myeloperoxidase; NAFLD, nonalcoholic fatty liver disease; NAS, NAFLD activity score; PA, palmitic acid; PGP, proline-glycine-proline; PREP, Prolyl endopeptidase; qRT-PCR, quantitative reverse transcription-polymerase chain reaction; ROS, reactive oxygen species; SREBP1, Sterol regulatory element-binding protein-1; Tβ4, thymosin β4; TBST, Tris buffered saline containing 0.1% Tween-20; TC, total cholesterol; TNF-α, tumor necrosis factor-alpha.

[#]Contributed equally to this work.

[*]**Correspondence to:** Jian-Gao Fan, Department of Gastroenterology, Xinhua Hospital, Shanghai Jiaotong University School of Medicine, 1665 Kongjiang Road, Shanghai 200092, China. ORCID: https://orcid.org/0000-0001-7443-5056. Tel/Fax: +86-21-25077340, Email: fanjiangao@xinhuamed.com.cn; Yuan-Wen Chen, Department of Gastroenterology, Huadong Hospital, Fudan University, 221 West Yan'an Road, Shanghai, 200040, China. ORCID: https://orcid.org/0000-0003-4210-007X. Tel/Fax: +86-21-62483180, E-mail: chenywhdgi@fudan.edu.cn

Introduction

Metabolic dysfunction-associated fatty liver disease (MAFLD), a new nomenclature for nonalcoholic fatty liver disease (NAFLD), was proposed to reflect the current understanding of fatty liver diseases associated with metabolic dysfunction.[1,2] MAFLD comprises a spectrum of liver histopathologies ranging from simple steatosis to steatohepatitis and more advanced stages, including fibrosis and cirrhosis, ultimately resulting in liver failure and hepatocellular carcinoma.[1] Currently, MAFLD has become a 'pandemic' posing a substantial health and economic burden to patients and society.[3,4]

Prolyl endopeptidase (PREP) is a serine endopeptidase that hydrolyzes peptide bonds at the proline carboxyl terminal.[5] Notably, numerous studies have suggested that in addition

to its earlier recognized enzymatic functions, PREP possesses nonenzymatic functions and participates in many pathological processes, such as inflammation, oxidative stress, and autophagy.[6] Furthermore, our previous studies found that PREP knockout could alleviate hepatic steatosis, inflammation, and oxidative stress in high-fat diet (HFD) or methionine-choline-deficient (MCD) diet-induced MAFLD models.[7,8] Therefore, we hypothesized that PREP inhibitors may be an effective pharmacological treatment for MAFLD. However, cumulative studies have suggested that PREP performs complex functions that vary according to the etiology and stage of the disease[9–12] and that PREP positively modulates inflammatory reactions.[9,10,13] The combined action of PREP and matrix metalloproteinases 8/9 (MMP8/9) cleaves collagen into proline-glycine-proline (PGP), a potent neutrophil chemoattractant and activator.[9] Moreover, PREP inhibition or knockout significantly suppresses PGP production and neutrophilic inflammation.[10,13] However, PREP also negatively modulates inflammatory reactions.[11,12,14] PREP may exhibit anti-inflammatory and antifibrotic effects through N-acetyl-seryl-aspartyl-lysyl-proline (AcSDKP), which is released from thymosin β4 (Tβ4) by the combined action of meprin α and PREP.[11] Our previous findings suggested a deficiency in endogenous AcSDKP could accelerate liver fibrosis progression in a carbon tetrachloride (CCl_4)-induced rat model.[12] Therefore, understanding the dynamic changes in PREP-PGP/AcSDKP, and clarifying its role and molecular mechanism in developing inflammatory diseases such as MAFLD, is the foundation for PREP intervention.

This study used the HFD-induced MAFLD model to explore dynamic changes in the PREP-PGP/AcSDKP system over time. In addition, we established another HFD-induced MAFLD mouse model and used a PREP inhibitor, KYP-2047, to examine whether the pharmacological blocking of PREP could exhibit the benefits shown in our previous PREP knockout studies,[7,8] and to further evaluate the possibility of using PREP inhibitors as therapeutic drugs for MAFLD.

Methods

Animal experiments

All animal handling and experimental procedures were approved by the Animal Care and Use Committee of Xinhua Hospital, affiliated with Shanghai Jiao Tong University School of Medicine. C57BL/6J mice were obtained from the Shanghai Experimental Animal Center (Shanghai, China) and housed five per cage in a specific pathogen-free facility with a 12:12 h light-dark cycle. After anesthesia, blood was obtained from the eyes of the mice, and they were euthanized by cervical dislocation. Liver tissue was either fixed in 4% paraformaldehyde or snap-frozen in liquid nitrogen and stored at −80°C until assayed.

Experiment 1: Mice were randomly divided into control and HFD groups. Control mice were fed a standard chow diet; HFD-mice were fed an HFD[7] including 88% standard diet, 10% lard, and 2% cholesterol (Trophi Feed High-tech Co., Ltd., Nantong, China). Forty control and 40 HFD-mice were used; 10 mice per group were sacrificed at 4, 8,12, and 16 weeks.

Experiment 2: Three groups of six mice each were included, controls, HFD, and HFD treated with KYP-2047 (HFD+KYP-2047). Control mice were fed a standard chow diet, while HFD and HFD+KYP-2047 were fed an HFD for 16 weeks. At the end of 10 weeks, the HFD+KYP-2047 group was infused with KYP-2047 (#SML0208; Sigma-Aldrich, St. Louis, MO, USA) diluted in 50% dimethylsulfoxide (DMSO) in saline at 5 mg/kg/day through a subcutaneous osmotic minipump (Alza Corp, Palo Alto, CA, USA) for 6 weeks, and the control and HFD model groups were infused with an equal amount of vehicle (50% DMSO) in saline, as previously described.[15,16] This dosage was used because previous pharmacokinetic study of KYP-2047[17] showed that a dose of 15 μmol/kg (5 mg/kg) exhibited extensive and long-lasting PREP inhibition in the liver for more than 12 h. Mice were sacrificed at 16 weeks.

Biochemical assays

Serum levels of aspartate aminotransferase (AST), alanine aminotransferase (ALT), alkaline phosphatase (ALP), total cholesterol (TC), low-density lipoprotein cholesterol (LDL-C), and fasting blood glucose (FBG) were assayed with an automated analyzer (Cobasc702; Roche, Basil, Switzerland). Fasting serum insulin levels were measured with an ultra-sensitive mouse insulin ELISA kit (#90080; Crystal Chem, Elk Grove Village, IL, USA) following the manufacturer's instructions. The homeostasis model assessment of insulin resistance (HOMA-IR) was calculated as fasting glucose (mM) × fasting insulin (mU/L)/22.5 as previously described.[18]

Liver catalase (CAT) and lactate dehydrogenase (LDH) levels were determined using commercially available kits (#A007-1-1 and #A020-1-2; Nanjing Jiancheng Bioengineering Institute, Nanjing, China). Hepatic reactive oxygen species (ROS) were determined using OxiSelect *in vitro* ROS/reactive nitrogen species assay kits (#STA-347; Cell Biolabs, San Diego, CA, USA) following the manufacturer's instructions.

Histological analysis

Formalin-fixed and paraffin-embedded liver tissues were cut into 6 μm sections, deparaffinized with xylene, and washed with absolute ethanol, followed by hematoxylin and eosin (HE) staining (#G1005; Servicebio, Wuhan, China) according to standard procedures.[19] The presence of neutrophils and macrophages in the liver was assessed by immunohistochemical staining as described previously.[20,21] Paraffin-embedded liver sections were incubated with CD68 antibody (#ab125212; Abcam, Cambridge, UK) or myeloperoxidase (MPO) antibody (#gb11224; Servicebio). The level of liver fibrosis was assessed by Masson's trichrome staining (#G1006; Servicebio) as previously described.[22,23] Liver fibrosis was evaluated based on the METAVIR classification (F0–F4): portal fibrosis without septa (F1), portal fibrosis with rare septa (F2), and numerous septa with and without cirrhosis (F3-4).[24] Moreover, mild fibrosis was defined as F1 or F2 and severe fibrosis as F3 or F4. The number of positive cells was calculated as the mean of the counts in six fields of view (×400).

NAFLD activity score (NAS)

Histological alterations were evaluated based on the NAS (range: 0–8).[25] Briefly, steatosis (quantity of lipid droplets) was scored as 0 (< 5%), 1 (5–33%), 2 (33–66%), or 3 (>66%). Lobular inflammation (foci of inflammatory cells) was scored as 0 (none), 1 (≤2 foci per 20 × magnification), or 2 (>2 foci per 20 × magnification). Hepatocyte ballooning was scored as 0 (none), 1 (few), or 2 (many).

Quantitative reverse transcription-polymerase chain reaction (qRT-PCR)

Total RNA was isolated from the liver using TRIzol reagent (#D9108B; Takara, Shiga, Japan), and reverse transcribed into cDNA using reverse transcriptase (#RR036A; Takara). qRT-PCR was performed using SYBR Premix Ex*Taq* (#RR420A; Takara) on a ViiA7 RT-PCR system (Applied Biosystems Inc., Waltham, MA, USA) following the standard SYBR Green pro-

tocol. All primer sequences are shown in Supplementary Table 1. Glyceraldehyde 3phosphate dehydrogenase (GAPDH) was used as the internal control. The relative mRNA expression for each gene was calculated as $2^{-\Delta\Delta Ct}$.

Western blotting

Liver tissues and HepG2 Cells were lysed with RIPA buffer (#P0013E; Beyotime) containing protease inhibitors (#ST506; Beyotime) and InStab phosphatase inhibitor cocktail (#20109ES05; Yeasen, Shanghai, China). Lysates were centrifuged (16,000 rpm, 15 m, 4°C), and the supernatant was collected, boiled in SDS sample buffer for 5–10 m, and separated by 8–12% SDS-PAGE. After that, proteins were transferred onto polyvinylidene fluoride membranes at 300 mA and blocked with 5% nonfat milk dissolved in Tris-buffered saline containing 0.1% Tween-20 (TBST) for 2 h. Membranes were incubated with primary antibodies overnight at 4°C, followed by washing with TBST three times for 5 m each, then incubated with HRP-conjugated secondary antibodies (#A0208 or # A0216; Beyotime). Signals were detected with the immobilon western chemiluminescent HRP substrate (#WBKLS0100; Millipore, Darmstadt, Germany), imaged with a ChemiDoc XRS+ system (Bio-Rad, Hercules, CA, USA), and quantified with Image Lab Version 2.0.1 (Bio-Rad). Primary antibodies against PREP (#ab58988; Abcam), MMP8 (#ab81286; Abcam), MMP9 (#ab38898; Abcam), meprin α (#AF4007; R&D Systems, Minneapolis, MN, USA), Tβ4 (#19850-1-AP, Proteintech), NF-κB phosphor-P65 (#3033T; Cell Signaling Technology, Danvers, MA, USA), phosphoERK1/2 (#4370T; Cell Signaling Technology), α-smooth muscle actin (α-SMA, #19245T; Cell Signaling Technology), Beclin1 (#3495T; Cell Signaling Technology), P62 (#ab109012' Abcam), and LC3II (#14600-1-AP; Proteintech, Rosemont, IL, USA) were used. GAPDH (#60004-1-Ig; Proteintech) was used as the loading control.

Liver and serum PREP activity

Approximately 100 mg of frozen liver tissue was homogenized with 500 μL of 10 mM Tris-HCl buffer (pH 7.4), followed by centrifugation (16,000 *g*, 20 m, 4°C). The supernatant was removed and used for subsequent experiments. The supernatant of liver homogenates (10 μL) or the serum samples (10 μL) was added to 465 μL Tris-HCl (10 mM, pH 7.4) and incubated at 30°C for 30 m. After that, 25 μL of substrate (4 mM Suc-Gly-Pro-AMC; Bachem, Bubendorf, Switzerland) was added and mixed gently. The reaction was incubated at 30°C for 60 m and terminated by adding 500 μL 1 M sodium acetate buffer (pH 4.2). The formation of AMC was determined by measuring the fluorescence intensity at 460 nm with excitation at 355 nm using Synergy H4 Plate Reader (BioTek, Winooski, VT, USA). The results of PREP activity were reported as pmol AMC/m/mg total protein.

Measurement of PGP

Approximately 50 mg of frozen liver tissue was sonicated with 800 μL of methanol/acetonitrile mixture (1:1, v/v) for 30 m at 4°C and placed in a −20°C freezer for 1 h followed by centrifugation (15,000 rpm, 30 m, 4°C). The supernatant was subjected to API5500 QQQ – MS and Waters Acquity UPLC systems (Waters Corp., Milford, MA, USA) under the below conditions. Ultra-performance liquid chromatography separation was performed on an ACQUITY UPLC BEH HILIC (100 mm × 2.1 mm, dp=1.7 μm) with a mobile phase of 0.2% formic acid and acetonitrile running at 0.7 mL/m. The positive electrospray mass transitions were monitored at 270>70 and 270>116 of PGP.

Measurement of AcSDKP

Liver AcSDKP concentration was measured using a highly sensitive and specific enzyme immunoassay kit (SPI-Bio and CEA, Fontenay-aux-Roses, France) following the manufacturer's protocol.[12]

Preparation of palmitic acid (PA) and KYP-2047

A PA-induced MAFLD cell model was established by exposing HepG2 cells to 0.25 mM PA for 24 h. PA powder (#P9767; Sigma-Aldrich, St. Louis, USA) was dissolved in sterile water supplemented with 1% fatty acid-free bovine serum albumin (BSA, #A8806; Sigma-Aldrich) at 70°C and filtered through a 0.22 μm filter to produce a 5 mM PA stock solution. Working PA solution was added to the cells at a concentration of 0.25 mM. A 100 mM KYP-2047 stock solution (#SML0208; Sigma-Aldrich) in DMSO was added to the HepG2 cell culture medium at a final working concentration of 10 μM (0.01% DMSO).

Cell culture and treatment

HepG2 human hepatoma cells were purchased from American Type Culture Collection and cultured in high-glucose DMEM (#C11995500BT; Gibco, Waltham, MA, USA), with 10% fetal bovine serum (# 04-001-1ACS; Biological Industries, Beit Haemek, Israel) at 37°C, 5% CO_2. When the cultures reached 70–80% confluence, they were exposed to different stimuli for 24 h to explore the effect of KYP-2047 (10 μM) on the 0.25 mM PA-induced MAFLD cell model. The cells were divided into four groups according to the following experimental conditions: control, KYP-2047, and PA with or without KYP-2047 treatment. Control reactions contained equivalent concentrations of DMSO and BSA.

Autophagy flux analysis

HepG2 cells were grown to 40–50% confluence in 12-well plates and transfected with Ad-mCherry-GFP-LC3B adenovirus (#C3011; Beyotime) at an MOI of 50 for 24 h. After two washes, infected HepG2 cells were treated with PA, KYP-2047, or a combination of PA and KYP-2047 for 24 h. After that, autophagy flux was observed under a fluorescence microscope (BX51; Olympus, Tokyo, Japan) and evaluated by calculating the number of yellow and red puncta.

Statistical analysis

The results were reported as means±SDs. Independent samples *t*-tests were used for two-sample comparisons, and one-way analysis of variance with Tukey's multiple comparisons tests was used to compare multiple samples. Statistical processing was performed using SPSS (version 20.0; IBM Corp., Armonk, NY, USA) software. A p-value of <0.05 was considered statistically significant.

Results

Increased PREP protein expression and activity during MAFLD development

To identify the potential molecular mechanisms by which PREP promotes MAFLD development, we established an HFD-induced MAFLD mouse model assessed at different time points using HE staining (Fig. 1A). First, we explored PREP protein expression in the livers of HFD-fed mice at different time points. PREP protein levels were significantly higher in HFD-fed mice than in control mice from 12 to 16 w (Fig. 1B, C). Furthermore, we assessed the biological activity of PREP in the serum and showed that serum PREP activity was significantly higher in HFD-mice than in control mice from week

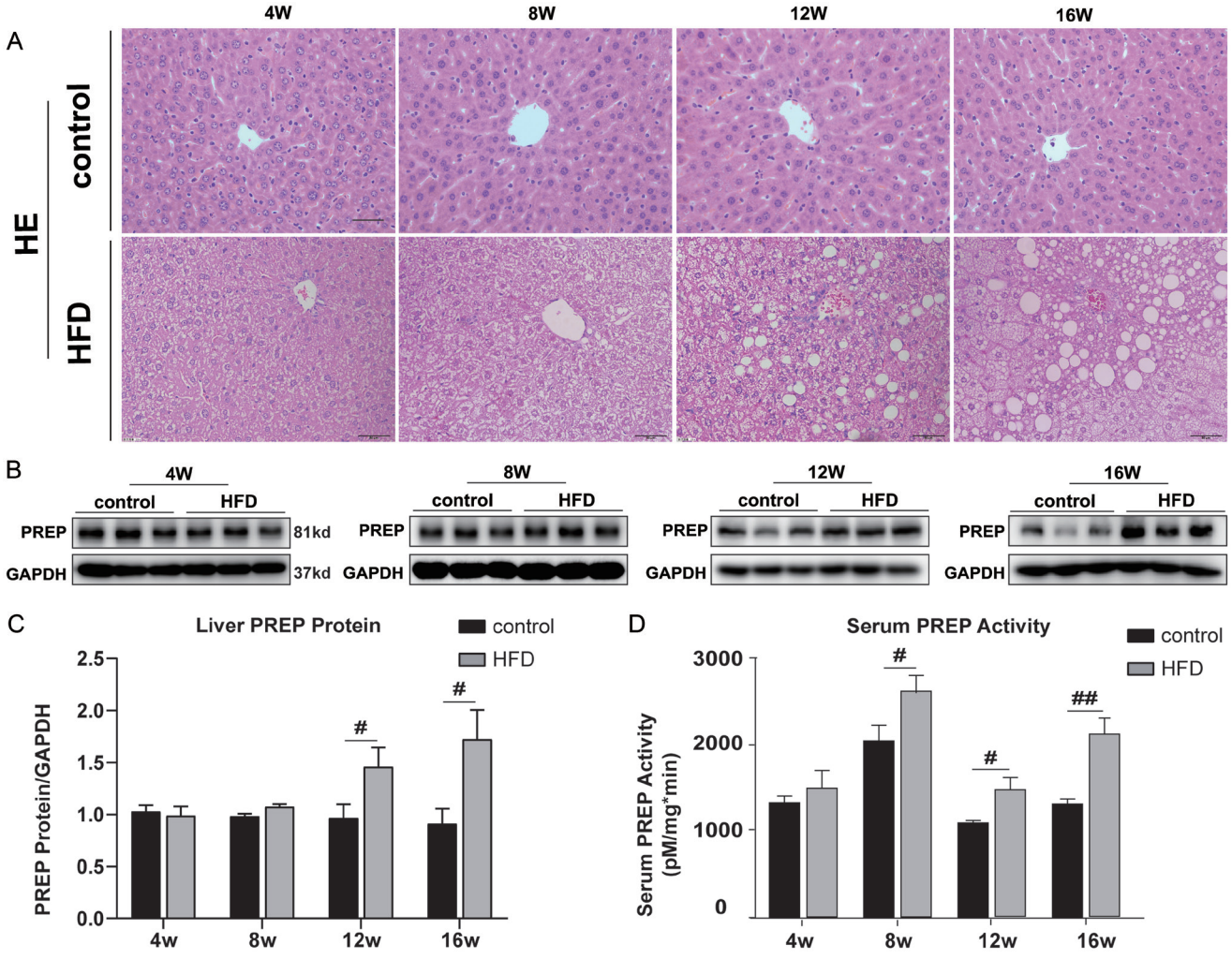

Fig. 1. Activity and protein expression of prolyl endopeptidase (PREP) was increased during metabolic dysfunction-associated fatty liver disease (MAFLD) development. (A) Hematoxylin-eosin (HE) staining in high-fat diet (HFD)-induced MAFLD mice model at different time points. (B-C) The expression of PREP protein in the liver of control and HFD-mice at different time points;(D) Serum PREP activity of control and HFD-mice at different time points; Data are means±SD (n=3–6). $^{\#}p<0.05$ and $^{\#\#}p<0.01$, control vs. HFD.

8 onwards, and the differences between groups were largest after 16 weeks (Fig. 1D).

MMP8/9-PREP-PGP axis was activated and the Tβ4-meprin α/PREP-AcSDKP axis was inhibited in livers of HFD-mice

During MAFLD development, our results showed that the MMP9 protein level in the liver was significantly increased in HFD-mice compared with that in the control mice at all time points (Fig. 2A–D). Significant differences in MMP8 protein levels between control and HFD-mice were observed at 8, 12, and 16 weeks (Fig. 2A–D). Correspondingly, we found that the production of PGP in HFD-mice was significantly increased compared to that in control mice after 16 weeks of HFD (Fig. 2E). The results suggested that PREP activity and protein levels in HFD-mice increased significantly compared with those in control mice during the development of MAFLD. However, we found that the Tβ4 protein, the substrate required for AcSDKP synthesis, was decreased in the livers of HFD-mice compared with control mice from 8–16 weeks (Fig. 2F–I). In addition, our study showed that meprin α, a crucial regulatory molecule of AcSDKP synthesis, was also decreased in the livers of HFD-mice from 8–16 weeks (Fig. 2F–I). The production of AcSDKP in HFD-mice was significantly lower than that in control mice after 16 weeks of HFD (Fig. 2J). Therefore, our results indicated that increased PREP activity and protein expression during MAFLD development mainly results in the activation of the MMP8/9-PREP-PGP axis rather than the Tβ4-meprin α/PREP-AcSDKP axis.

PREP inhibitor attenuated HFD-induced liver injury and oxidative stress

To identify whether inhibiting PREP reversed MAFLD pathologies, the PREP inhibitor, KYP-2047, was administered to HFD-mice. As expected, PREP activity in the serum and liver tissue was significantly inhibited after 6 weeks (Fig. 3A, B). As shown in Figure 3C, HE staining of liver sections demonstrated that KYP-2047 treatment reduced HFD-induced hepatic lipid accumulation and the infiltration of inflammatory cells. Furthermore, HFD+KYP-2047 mice displayed significantly lower NAS than HFD-mice (Table 1). Serum markers of liver function, such as ALT (Fig. 3D), AST (Fig. 3E), and ALP (Fig. 3F), were

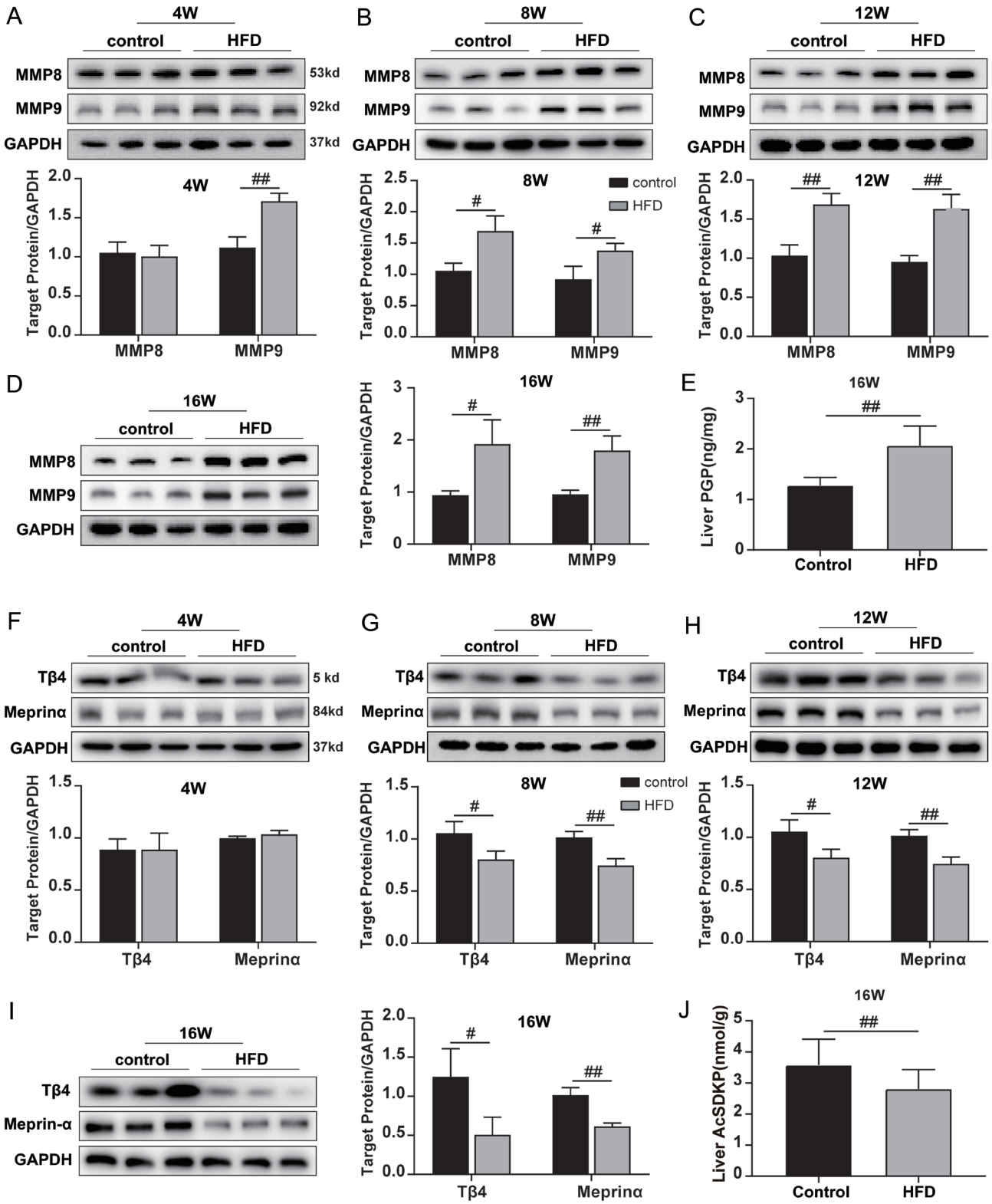

Fig. 2. The PREP-proline-glycine-proline (PGP)/N-acetyl-seryl-aspartyl-lysyl-proline (AcSDKP) system was developing in the direction of proinflammatory matrix metalloproteinases 8/9 (MMP8/9)-PREP-PGP during MAFLD development. (A-D) Protein expression of MMP8 and MMP9 in the liver of control and HFD-mice at different time points. (E) The PGP level in the control liver and HFD-mice at 16 weeks. (F-I) Protein expression of meprin α and thymosin-β4 (Tβ4) in the liver of control and HFD-mice at different time points. (J) The level of AcSDKP in the liver of control and HFD-mice at 16 weeks; Data are means±SD (n=3–6). $^{\#}p<0.05$ and $^{\#\#}p<0.01$, control vs. HFD.

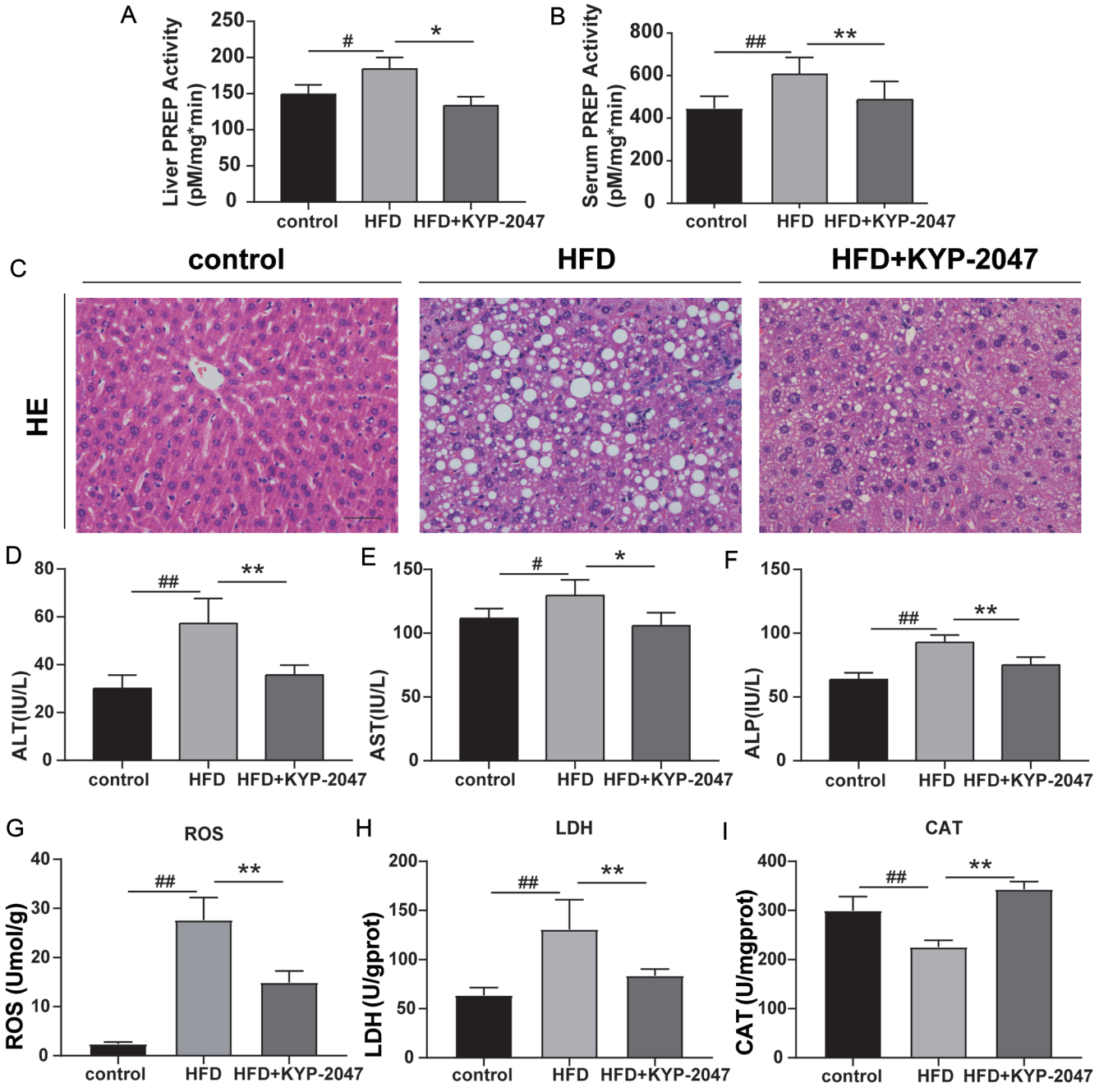

Fig. 3. PREP inhibitor improved hepatic pathology and serological indicators of liver function in HFD-induced MAFLD. (A, B) Liver PREP and serum PREP activity in control, HFD, and HFD+KYP-2047 mice. (C) HE staining of representative samples from control, HFD, and HFD+KYP-2047 mice. (D) Alanine aminotransferase (ALT) in each group. (E) Aspartate aminotransferase (AST) in each group. (F) Alkaline phosphatase (ALP) in each group. (G–I) Reactive oxygen species (ROS), lactate dehydrogenase (LDH), and catalase (CAT) are in each group. Data are means±SDs (n=5–6). $^{\#}p<0.05$ and $^{\#\#}p<0.01$, control vs. HFD; $^{\#}p<0.05$ and $^{\#\#}p<0.01$, HFD vs. HFD+KYP-2047.

Table 1. Comparison of NAFLD activity score (NAS) in each group

Group	Steatosis	Lobular inflammation	Ballooning	NAS
Control	0	0	0	0
HFD	2.00±0.71$^{\#\#}$	2.75±0.43$^{\#\#}$	1.00±0.00$^{\#\#}$	5.75±1.09$^{\#\#}$
HFD+KYP-2047	1.00±0.00**	1.00±0.71**	1.00±0.00	3.00±0.71**

Data are means±SDs (n=6). $^{\#}p<0.05$ and $^{\#\#}p<0.01$, control vs. HFD; $^{*}p<0.05$ and $^{**}p<0.01$, HFD vs. HFD+KYP-2047.

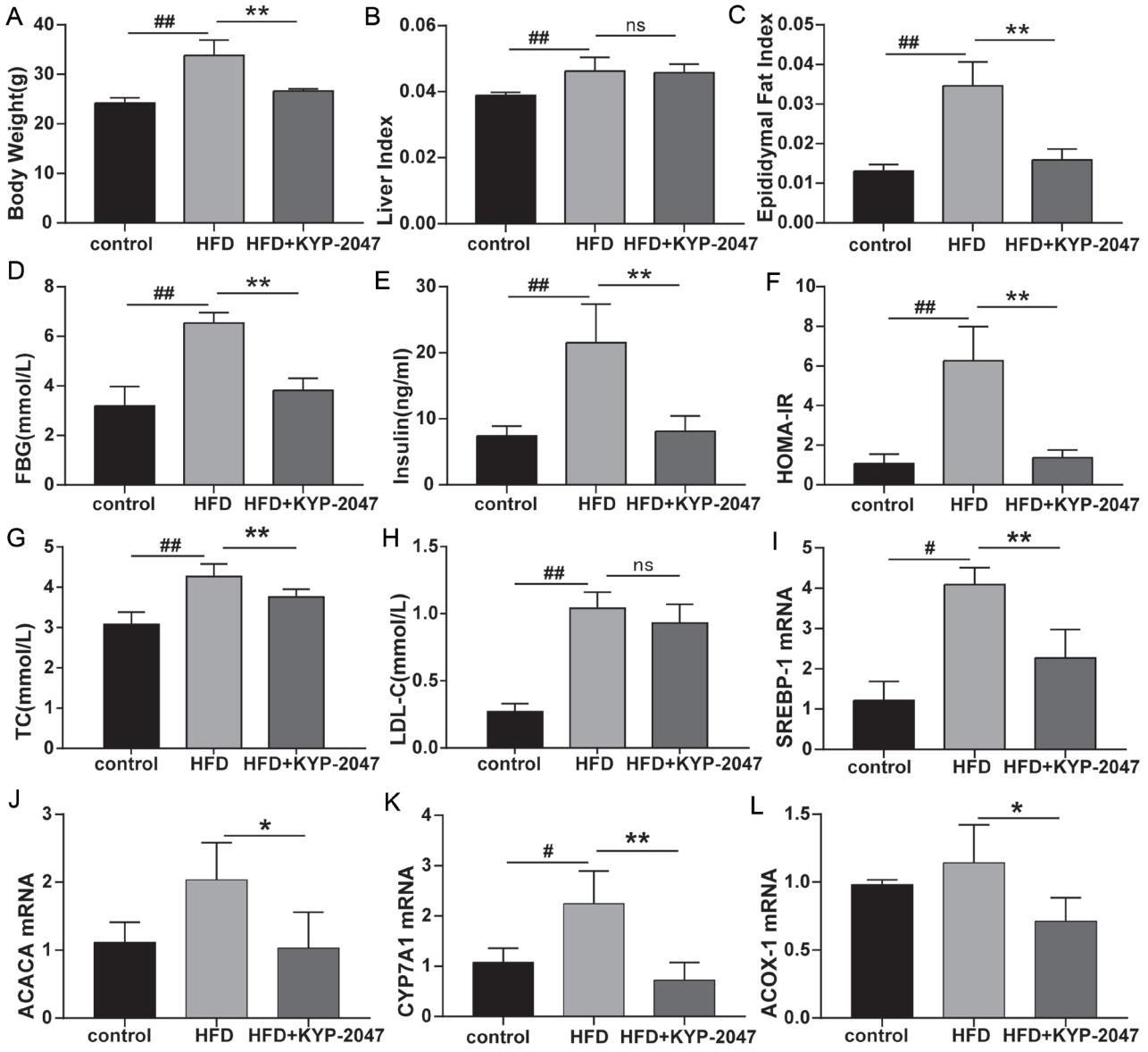

Fig. 4. PREP inhibitor ameliorated HFD-induced liver injury and metabolic abnormalities. (A) Body weight in each group. (B) Liver index (liver weight/body weight) in each group. (C) Epididymal fat index (epididymal fat weight/body weight) in each group. (D) Fasting blood glucose (FBG) in each group. (E) Insulin in each group. (F) Homeostatic model assessment of insulin resistance (HOMA-IR) in each group. (G-H) serum total cholesterol (TC)and low-density lipoprotein cholesterol (LDL-C) in each group. (I-L) mRNA expression of Sterol regulatory element-binding protein-1 (SREBP1), acetyl CoA carboxylase-alpha (ACACA), cholesterol 7-alpha hydroxylase (CYP7A1), and acyl-coenzyme A oxidase1 (ACOX1). Data are means±SDs (n=3–6 $^{\#}p$<0.05 and$^{\#\#}p$<0.01, control vs. HFD; *p<0.05 and **p<0.01, HFD vs. HFD+KYP-2047.

significantly decreased in the HFD+KYP-2047 mice compared with those in the HFD-mice. More important, KYP-2047 treatment improved HFD-induced oxidative stress. As shown in Figures 3G and H, ROS and LDH levels were higher in the livers of HFD-mice than those in control mice, indicating that the HFD could induce hepatic oxidative stress. However, ROS and LDH levels in HFD-mice were significantly reduced after KYP-2047 treatment. Moreover, CAT antioxidant levels were significantly higher in the livers of HFD+KYP-2047 mice than in those of HFD-mice (Fig. 3I).

PREP inhibitor attenuated HFD-induced aberrant glycolipid metabolism

As shown in Figure 4A–C, HFD+KYP-2047 mice gained less body weight and had a lower epididymal fat index than HFD-mice, but the liver index was similar between the two groups. HFD+KYP-2047 mice exhibited a significant improvement in glucose metabolism indexes (e.g., FBG, insulin, and HOMA-IR) compared to HFD-mice (Fig. 4D–F). Although there was no difference in serum LDL-C levels between HFD-mice and HFD+KYP-2047 mice (Fig. 4H), serum TC was significantly lower in HFD+KYP-2047 mice than in HFD-mice (Fig. 4G). Furthermore, KYP-2047 treatment down-regulated the expression of lipogenic genes, sterol regulatory element-binding protein-1 (SREBP1; Fig. 4I) and acetyl CoA carboxylase-alpha (ACACA; Fig. 4J), and *de novo* synthesis of the bile acid gene, cholesterol 7-alpha hydroxylase (CYP7A1; Fig. 4K), induced by HFD feeding. Moreover, KYP-2047 treatment im-

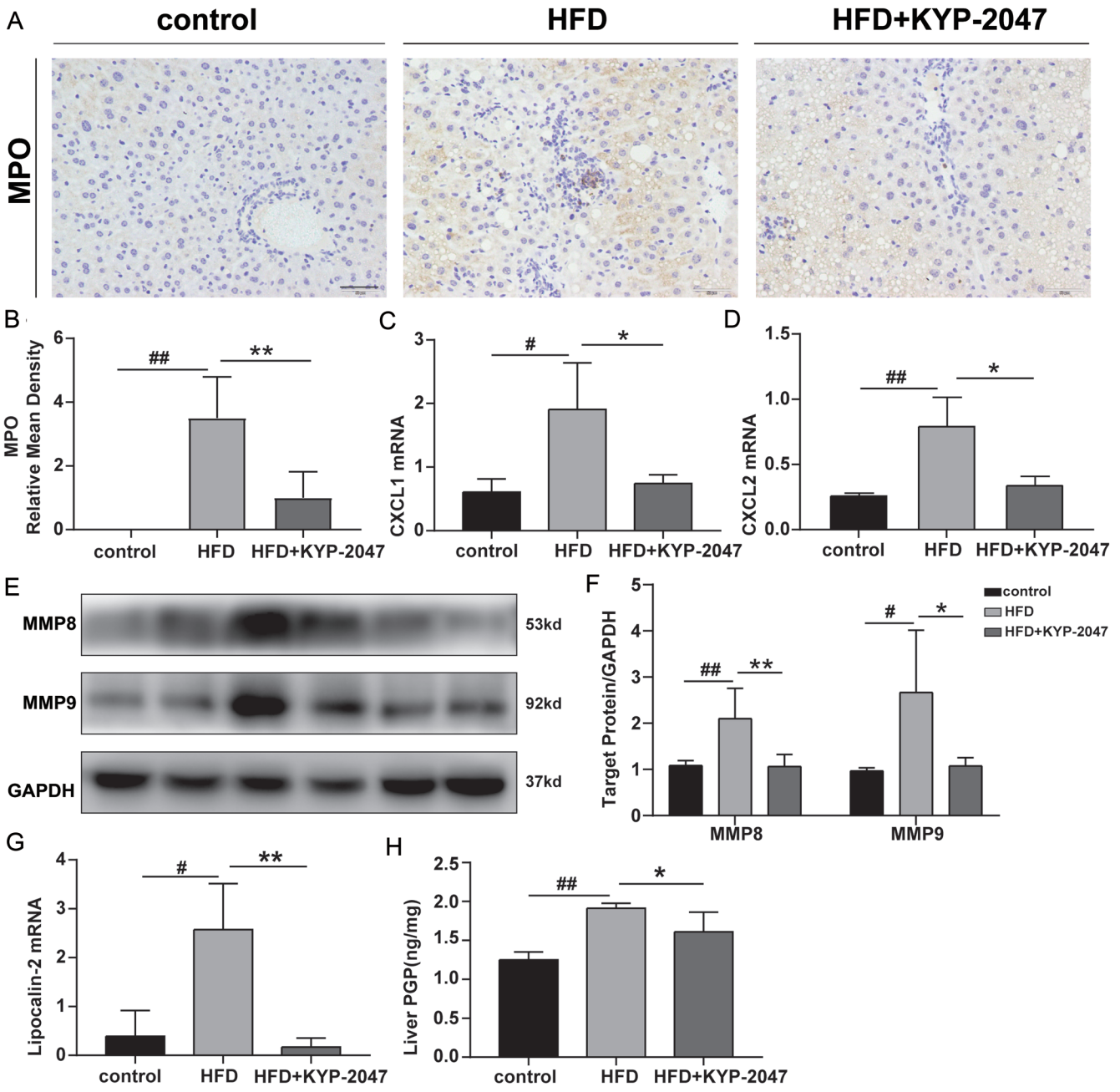

Fig. 5. PREP inhibitor restrained the activation of MMP8/9-PREP-PGP axis and reduced hepatic neutrophil accumulation. (A) The representative images of myeloperoxidase (MPO) immunohistochemical staining in liver samples from each group (scale bar, 50 μm). (B) MPO-positive cell counts. (C-D) mRNA expression of CXCL1 and CXCL2. (E) Protein expression of matrix metalloproteinase (MMP) 8, MMP9, and GAPDH. (F) The relative ratio of protein (MMP8 and MMP9) to GAPDH. (G) mRNA expression of Lipocalin-2 (LCN2). (H) The level of PGP in the liver of each group. Data are means±SDs (n=3). $^{\#}p$<0.05 and $^{\#\#}p$<0.01, control vs. HFD; $^{*}p$<0.05 and $^{**}p$<0.01, HFD vs. HFD+KYP-2047.

proved the impairment of fatty acid β-oxidation gene, acyl-coenzyme A oxidase 1 (ACOX1), induced by HFD (Fig. 4L).

PREP inhibitor decreased HFD-induced neutrophil by inhibiting MMP8/9 and PGP

Immunohistochemistry was performed for the neutrophil marker, MPO, to analyze inflammatory cell infiltration into liver tissue. We found that the number of neutrophils in HFD, but not HFD + KYP-2047, mouse liver was significantly increased (Fig. 5A, B). Similarly, the mRNA expression levels of Lipocalin-2 (LCN-2), another neutrophil activation marker, were significantly decreased in HFD+KYP-2047 mice compared to HFD-mice (Fig. 5G). Furthermore, KYP-2047 significantly down-regulated the expression of genes associated with neutrophil chemotaxis (e.g., CXCL1 and CXCL2) induced by HFD (Fig. 5C, D). Moreover, serum and liver tissue PREP activity increased significantly after 16 weeks of HFD. However, this was down-regulated by a 6-week period of KYP-2047 treatment.

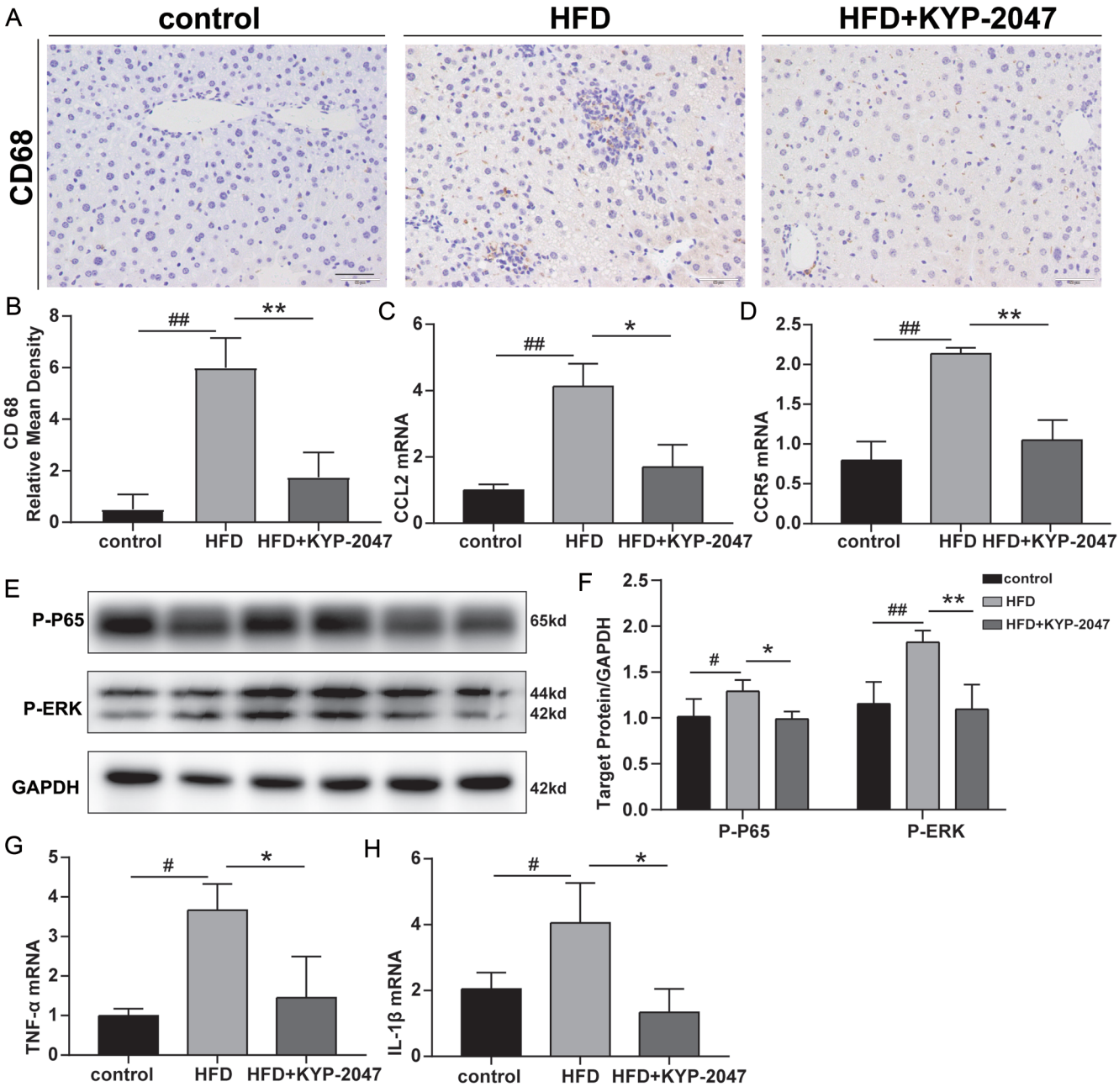

Fig. 6. PREP inhibitor reduced hepatic macrophage accumulation and inflammation. (A) The representative images of CD68 immunohistochemical staining in liver samples from each group (scale bar, 50 μm). (B) CD68-positive cell counts. (C-D) mRNA expression of CCL2 and CCR5. (E) Protein expression of P-P65, P-ERK, and GAPDH. (F) The relative ratio of protein (P-P65 and P-ERK) to GAPDH. (G-H) mRNA expression of tumor necrosis factor-alpha (TNF-α) and interleukin-1β (IL-1β). Data are means±SDs (n=3). $^{\#}p$<0.05 and $^{\#\#}p$<0.01, control vs. HFD; $^{*}p$<0.05 and $^{**}p$<0.01, HFD vs. HFD+KYP-2047.

Additionally, the MMP8 and MMP9 protein levels in the livers of HFD-mice were significantly increased after 16 weeks of HFD feeding, which could be reduced by treatment with KYP-2047 (Fig. 5E, F). More importantly, we demonstrated that subcutaneous injection of KYP-2047 for 6 weeks significantly reduced the production of PGP induced by HFD feeding (Fig. 5H).

PREP inhibitor decreased HFD-induced macrophage accumulation and hepatic inflammation

Paraffin-embedded liver sections immunostained with macrophage-specific CD68 antibodies to analyze macrophage cell infiltration, showed that the HFD caused a significant accumulation of macrophages. However, KYP-2047 treatment significantly reduced HFD-induced macrophage cell infiltration (Fig. 6A, B). In addition, we found that KYP-2047 significantly down-regulated the expression of genes associated with HFD-induced macrophage chemotaxis (e.g., CCL2 and CCR5) (Fig. 6C, D). Accordingly, the expression of inflammation-related proteins (e.g., P-ERK and P-P65) (Fig. 6E, F) and genes, e.g., interleukin-1β (IL-1β) and tumor necrosis

factor-alpha (TNF-α; Fig. 6G, H) was significantly lower in HFD+KYP-2047 mice than in HFD-mice.

Although current evidence suggests that PREP inhibitors have multiple anti-metabolic and anti-inflammatory properties, the levels of AcSDKP, an antifibrotic small molecule, were further decreased by using KYP-2047 in HFD-mice (Supplementary Fig. 1A). Therefore, we investigated the effect of KYP-2047 on HFD-induced liver fibrosis. Masson's trichrome staining showed that HFD feeding induced hepatic fibrosis. Briefly, all HFD-mice were in the mild fibrosis stage; 50% (3/6) had F1 fibrosis, and 50% (3/6) had F2 fibrosis. More importantly, KYP-2047 treatment did not exacerbate HFD-induced fibrosis. HFD+KYP2047 mice maintained a fibrosis score of F1/F2, 66.7% (4/6) had F1 fibrosis, and 33.3% (2/6) had F2 fibrosis (Supplementary Fig. 1B). Meanwhile, KYP-2047 treatment induced a significant decrease in the expression of profibrotic marker α-SMA in HFD+KYP-2047 mice compared to HFD-mice (Supplementary Fig. 1C, D). However, there was no difference in the mRNA expression levels of collagen type I alpha 1 chain (COL1A1) and collagen type III alpha 1 chain (COL3A1) between HFD and HFD+KYP-2047 mice (Supplementary Fig. 1E, F).

PREP inhibitor ameliorated impaired autophagy in the liver of HFD-mice and PA-exposed HepG2 cells

Autophagy indicator (Beclin1 and LC3BII) levels were lower in HFD-mice than in control mice (Fig. 7A, B). However, KYP-2047 treatment increased hepatic LC3II and Beclin1 levels in HFD-fed mice. Because the reduction of P62 is considered a marker of autophagic flux activation and vice versa,[26] we measured the P62 protein expression levels. Our results showed that P62 protein levels significantly increased after a 16-week HFD, whereas they were downregulated by a 6-week period of KYP-2047 treatment (Fig. 7A, B). To further clarify the association between PREP and autophagy, we evaluated whether inhibiting PREP ameliorates PA-induced impaired autophagy in HepG2 cells. We found that LC3II was increased after PA stimulation for 24 h, and KYP-2047 treatment further increased the LC3II level in the PA+KYP-2047 group compared with the PA group (Fig. 7F). This appears to contradict our *in vivo* results, but, in general, autophagy consists of two steps, formation and degradation of autophagosomes.[27] Thus, increased LC3II may result from either increased autophagosome formation or suppressed degradation of autophagosomes. HepG2 cells were infected with mCherry-GFP-LC3 adenovirus to monitor autophagy flux in the presence of PA and/or KYP-2047. Using this probe, we could distinguish between autophagosomes (GFP+/mCherry+, yellow dots) and autolysosomes (GFP−/mCherry+, red dots). Under normal conditions, the mCherry-GFP-LC3B fusion protein displayed a diffuse cytoplasmic distribution and homogeneous yellow fluorescence (Fig. 7C). Treatment with PA for 24 h resulted in a significant increase in yellow dots compared with the control group (Fig. 7C). However, PA+KYP-2047 treatment led to a significant increase in the number of red dots and a decrease in the number of yellow dots compared with PA treatment alone (Fig. 7C). Briefly, autophagy was initiated after HepG2 cells were treated with PA alone or PA+KYP-2047. Moreover, 24-h PA treatment suppressed the process of the autophagy-lysosome pathway, while KYP-2047 improved the above pathway and restored autophagic flux. Consistent with this, treatment with PA significantly increased the P62 protein levels, and KYP-2047 significantly inhibited PA-induced P62 accumulation (Fig. 7E). In addition, Beclin1 levels (Fig. 7D) were significantly upregulated in the PA+KYP-2047 group compared with those in the PA group, further indicating the benefits of KYP-2047 related to autophagy.

Discussion

In this study, we first used an HFD-induced MAFLD mouse model at different times (4, 8, 12, and 16 weeks) to explore the dynamic changes in the PREP-PGP/AcSDKP system during MAFLD initiation and development. We demonstrated that PREP activity and protein expression in the HFD group were both significantly higher than those in the control group from the 12th week onwards, and the maximum difference was in the steatohepatitis stage (16 weeks HFD). The increased PREP activity and protein levels mainly result in the activation of the MMP8/9-PREP-PGP axis rather than the Tβ4-meprin α/PREP-AcSDKP axis. Thus, in another experiment, mice received a 16-week HFD to induce steatohepatitis and were then treated with the PREP inhibitor, KYP-2047. We demonstrated that KYP-2047 treatment reduced HFD-induced liver injury, oxidative stress, dysglycemia, and dyslipidemia; improved lipid metabolism by suppressing lipogenesis genes and inducing β-oxidation-related genes; alleviated hepatic fat accumulation; attenuated hepatic inflammation and inflammatory cell infiltration by decreasing MMP8/9 and PGP; and ameliorated impaired autophagy *in vivo* and *in vitro,* thus contributing to the improvement of HFD-induced MAFLD in mice (Fig. 8).

PREP activity and protein levels changed dynamically during MAFLD development in the dynamic models of HFD-fed mice. Specifically, no statistical difference in PREP activity and protein expression was observed between the control and HFD-mice in the simple steatosis stage (4 weeks HFD). However, as the model developed further, we found that PREP activity and protein expression in the HFD group were both significantly higher than those in the control group from the 12th week onwards, with the maximum difference observed in the steatohepatitis stage (16 weeks HFD). A recent study reported that PREP could not be seen in microglial cells (macrophage-like cells) in the brain under normal circumstances, but the expression and activity of PREP in microglia were significantly increased after immunoglobulin G activation.[28] Similarly, recent studies have shown that lipopolysaccharide and interferon-gamma can induce microglia to secrete PREP and enhance its activity.[29] Notably, PREP is highly active in the liver, mainly in hepatocytes.[30,31] We therefore speculate that hepatocyte damage and activated macrophages may be the reason for the increase in PREP activity and protein levels during the development of MAFLD. In the early stage of MAFLD (simple steatosis), the number of damaged hepatocytes and activated macrophages (M1 macrophages) was low; therefore, there was no significant difference in PREP activity and protein levels in the serum and liver. When MAFLD progresses to steatohepatitis, the number of damaged hepatocytes and activated macrophages increases significantly, causing increased PREP expression in the liver, and promoting the release of intracellular PREP into the serum.

What role does PREP play in MAFLD development? Previous studies have shown that the synergy between PREP and MMP8/9 can cleave collagen into the neutrophil chemoattractant PGP in inflammatory diseases.[9,10] As expected, in addition to the increased PREP activity during MAFLD development described above, we also found that the expression of MMP8/9 protein in HFD-mice was significantly higher than that in control mice from 8 to 16 weeks. Furthermore, we showed that the neutrophil chemoattractant PGP was significantly increased in HFD-mice compared to that in control

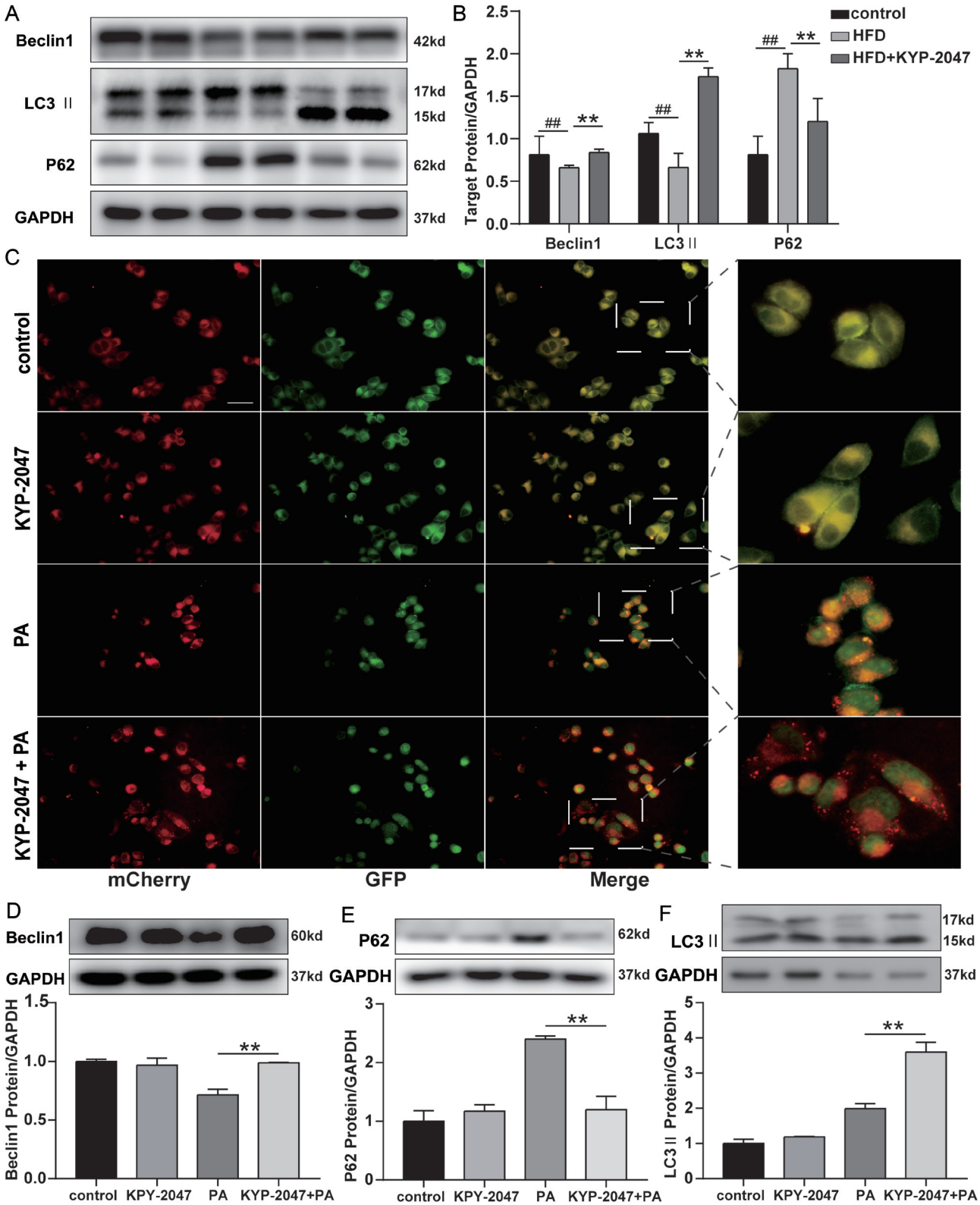

Fig. 7. PREP inhibitor can improve impaired autophagy *in vivo* and *in vitro*. (A) Protein expression of Beclin1, LC3II, P62, and GAPDH in the liver of control, HFD, and HFD+KYP-2047 mice. (B) The relative ratio of protein (Beclin1, LC3II, and P62) to GAPDH. (C) Representative images of HepG2 cells transfected Ad-mCherry-GFP-LC3B adenovirus after palmitic acid (PA, 200 μM, 24 h) or KYP-2047 treatment (10 μM, 24 h). (D-F) Protein expression of Beclin1, P62, LC3II, and GAPDH in HepG2 cells. Data are means±SDs (n=3). $^{\#}p<0.05$ and $^{\#\#}p<0.01$, control vs. HFD; $^{*}p<0.05$ and $^{**}p<0.01$, HFD vs. HFD+KYP-2047; $^{\#}p<0.05$ and $^{\#\#}p<0.01$, control vs. PA.

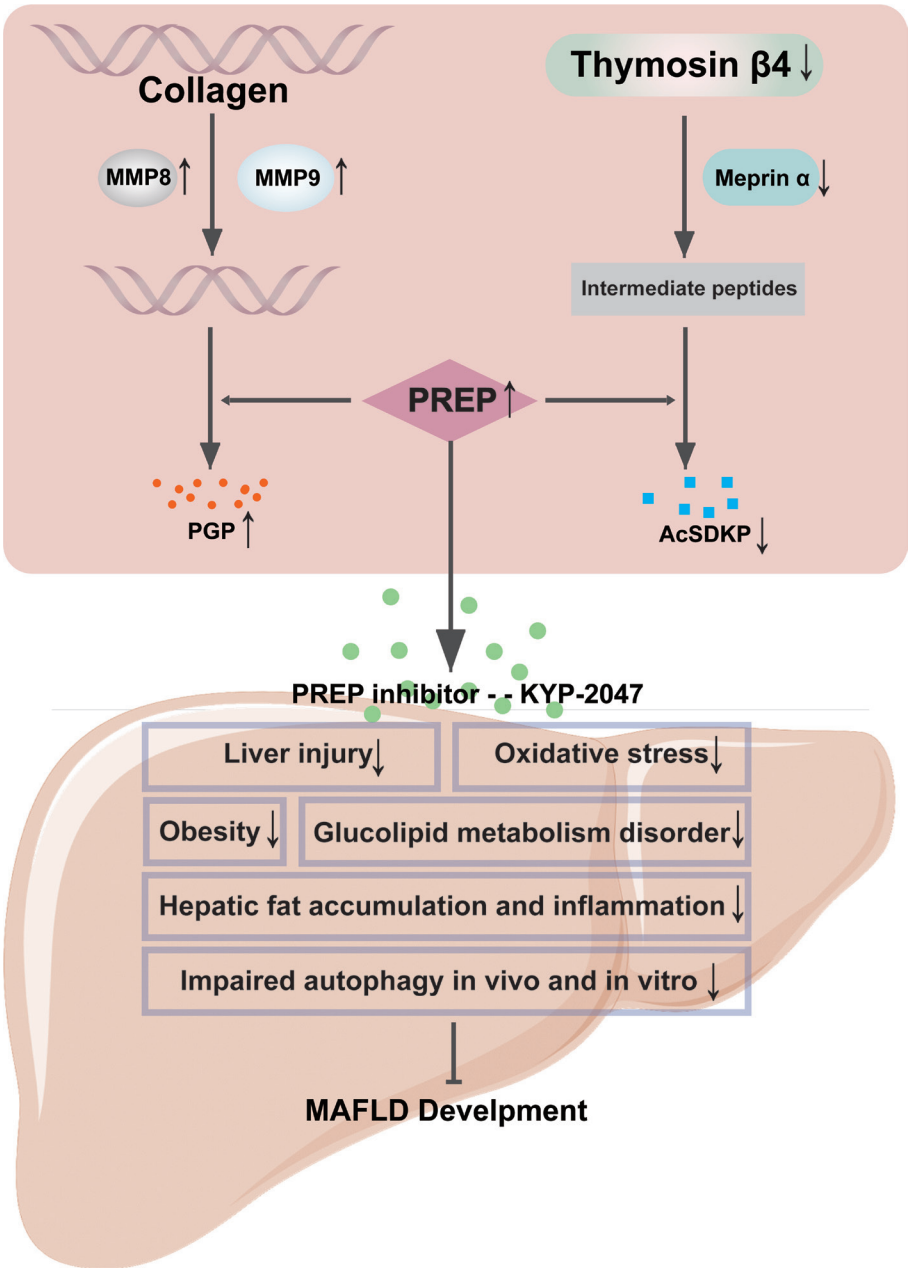

Fig. 8. The PREP-PGP/AcSDKP system was developing in the direction of proinflammatory MMP8/9-PREP-PGP during MAFLD development, and PREP inhibitor exerted beneficial effects on MAFLD. In MMP8/9-PREP-PGP axis, MMP8/9 can cleave collagen into small fragments first. Then, these small collagen fragments are cleaved into PGP by PREP. During MAFLD development, increased PREP activity and MMP 8/9 expression positively contribute to the production of PGP. In Tβ4-meprin α/PREP-AcSDKP axis, meprin α hydrolyzes Tβ4 into terminal intermediate peptide first. Then, the intermediate peptide serves as the substrate for PREP in releasing AcSDKP. During MAFLD development, although PREP activity was increased, the production of AcSDKP was still decreased due to the lack of its substrate thymosin β4 and enzyme meprin α. Therefore, increased PREP activity in MAFLD development mainly results in activating MMP8/9-PREP-PGP axis rather than Tβ4-meprin α/PREP-AcSDKP axis. In addition, PREP inhibitor – KYP-2047 could reduce HFD-induce liver injury and oxidative stress, improve dysglycemia and dyslipidemia, alleviate hepatic fat accumulation and inflammation, and restore impaired autophagy in the livers of HFD-mice and PA-exposed HepG2 cells, thus stopping MAFLD development.

mice at 16 weeks. These data show that the proinflammatory MMP8/9-PREP-PGP system is activated during MAFLD development. However, it is worth noting that PREP not only increases the production of proinflammatory PGP but also increases the production of antifibrotic and anti-inflammatory AcSDKP, which is released from Tβ4 by the combined action of meprin α and PREP.[11] Here, we found that although PREP activity increased after 16 weeks of HFD, AcSDKP production decreased due to the lack of substrate, Tβ4, and enzyme, meprin α. Therefore, our results indicate that increased PREP activity in MAFLD development mainly resulted in the activation of the MMP8/9-PREP-PGP axis rather than the Tβ4-meprin α/PREP-AcSDKP axis, suggesting that increased PREP activity could accelerate the transition from simple steatosis to steatohepatitis and that PREP inhibition should be considered as an intervention in the early stage of MAFLD.

MAFLD is the most common chronic liver disease worldwide.[3] However, because of a lack of effective drug therapy, lifestyle modifications are usually the first choice interventions.[32] Recently, we established PREP-KO mice using CRISPR/Cas9 technology and found that PREP knockout may improve hepatic steatosis, oxidative stress, and inflammatory responses in MAFLD mice.[7,8] Thus, in this study, we aimed to examine whether the pharmacological blocking of PREP can perform the above role, and evaluate the possibility of using PREP inhibitors as therapeutic drugs for MAFLD.

First, we demonstrated that PREP inhibition protects against liver injury. HFD+KYP-2047 mice displayed decreased NAS and improved liver function (ALT, AST, and ALP) compared to HFD-mice. More importantly, our results showed that KYP-2047 treatment protected the liver from HFD-induced oxidative stress damage. The indicators of oxidative stress in the livers of HFD+KYP-2047 mice were significantly reduced compared to those in HFD-mice. Concomitantly, the antioxidant enzymatic activity of CAT was higher in the livers of HFD+KYP-2047 mice than in HFD-mice, which was similar to our previous results in PREP-KO mice.[8]

Evidence indicates that PREP and its subfamily members are associated with metabolic status.[33,34] Moreover, our previous study showed that PREP knockout protects against HFD-induced abnormalities in glucose and lipid metabolism.[7] Those findings were consistent with our present findings that KYP-2047 reduced physical parameters (body weight and epididymal fat index), serum lipid content (TC), and indicators of glucose metabolism (FBG, insulin, and HOMA-I) in HFD-fed mice. Moreover, our present results suggest that PREP inhibition can reduce hepatic fat accumulation through inhibiting lipogenesis genes and enhancing β-oxidation genes, which might further explain the effect of PREP inhibition on histological improvement in the liver.

Hepatic inflammation is a pivotal feature in the pathogenesis of MAFLD, and determines the transition from steatosis to steatohepatitis.[35] Cumulative studies have shown that PREP activity and expression are significantly increased in inflammatory diseases,[36–39] and that PREP knockout or inhibition could alleviate inflammation.[29,33,38] Moreover, our previous studies also suggested that PREP knockout could alleviate inflammation, either in HFD-induced or MCD diet-induced MAFLD models.[7,8] As expected, we found that PREP inhibitors improved HFD-induced hepatic inflammation. Specifically, in addition to the potent inhibitory effect of KYP-2047 on the MMP8/9-PREP-PGP system, KYP-2047 also reduced the expression of other hepatic neutrophil and macrophage chemokines induced by HFD. Accordingly, a reduction in the number of hepatic macrophages and neutrophils was observed in HFD+KYP-2047 mice compared to that in HFD-mice. Furthermore, our results showed that KYP-2047 inhibited ERK and P65 phosphorylation and reduced transcription of proinflammatory genes, such as TNF-α and IL1β.

Although current evidence suggests that PREP inhibitors have multiple anti-metabolic and anti-inflammatory properties, we found that AcSDKP, an antifibrotic small molecule, was further decreased by KYP-2047 in HFD-mice. Therefore, we investigated the effect of KYP-2047 on HFD-induced liver fibrosis. KYP-2047 treatment did not exacerbate HFD-induced fibrosis but did induce a significant decrease in the expression of the profibrotic marker α-SMA in HFD+KYP-2047 mice compared to HFD-mice. Although seemingly contradictory, these two findings may not be mutually exclusive. It is well-established that liver fibrosis progression is a complex process involving multiple factors and cells.[40] Hepatic inflammation and oxidative damage are thought to be key factors in the development of fibrogenesis.[40,41] We therefore speculated that the benefits, such as anti-inflammatory and antioxidant stress, derived from short-term KYP-2047 treatment, outweigh the side effect of AcSDKP insufficiency. Accordingly, we did not observe progression of liver fibrosis in HFD-induced MAFLD mice after KYP-2047 treatment. However, 16 weeks of HFD feeding is insufficient to drive advanced fibrosis in mice.[42] Further studies should be performed to explore the relationship between PREP knockout/inhibition and hepatic fibrosis in different liver fibrosis models.

Numerous studies have suggested that PREP is a negative regulator of autophagy, and PREP inhibition or knockout can improve a series of human diseases by enhancing autophagy.[6,16,43–45] Notably, impaired autophagy is associated with the development of MAFLD.[46–48] We hypothesized that the PREP inhibitor, KYP-2047, contributes to the improvement of MAFLD by regulating autophagy. Here, we found that inhibition of PREP could improve impaired autophagy by increasing LC3II and beclin1 levels, P62 decreasing levels. Moreover, KYP-2047 increased autophagy flux in PA-exposed HepG2 cells, further verifying the relationship between PREP inhibition and autophagy. The improvement in autophagy has a beneficial role in ameliorating insulin resistance, abnormal lipid metabolism, and hepatic inflammation.[49] Therefore, we speculated that the ameliorative effects of KYP-2047 in the HFD-induced MAFLD model were mediated by either a direct protective effect of autophagy, or an indirect effect of autophagy, by modulating hepatic steatosis and inflammation.

This study has some limitations. First, PREP expression was measured in an animal model, which needs further exploration in human samples. Second, the effect of PREP inhibitor treatment on the progression of MAFLD, especially steatohepatitis with advanced fibrosis and cirrhosis, was not excluded from this study. However, the present results show that short-term AcSDKP deficiency caused by KYP2047 did not play a profibrotic role in HFD-induced MAFLD. Third, the exact mechanism of PREP inhibition on glucose and lipid metabolism has yet to be fully elucidated and needs to be further investigated in future studies.

Conclusions

In conclusion, we demonstrated that increased PREP activity in MAFLD development resulted in activation of the MMP8/9-PREP-PGP axis. Moreover, the PREP inhibitor, KYP-2047, attenuated hepatic steatosis, oxidative stress, inflammation, and impaired autophagy in an HFD-induced MAFLD model and showed good potential as a therapeutic drug for MAFLD treatment at least in a specific stage of the disease. However, this study was conducted in an animal model, and the application of PREP inhibitors in clinical treatment remains challenging. Further clinical studies are warranted before the PREP inhibitors are used for MAFLD treatment.

Funding

This work was financially supported by grants from the National Natural Science Foundation of China (81970511, 82270620).

Conflict of interest

JGF has been an associate editor of *Journal of Clinical and Translational Hepatology* since 2013. The other authors have no conflict of interests relevant to this publication.

Author contributions

Conceptualization, (JBZ, MTL, JGF, YWC), methodology (JBZ,

MTL, SZL, YQC), formal analysis (JBZ, MTL), investigation (JBZ, MTL, SZL, YQC), data curation (JBZ, MTL, JGF, YWC), writing–original draft preparation (JBZ, JGF, YWC), supervision (JGF, YWC), funding acquisition (YWC).

Ethical statement

All animal handling and experimental procedures were approved by the Animal Care and Use Committee of Xinhua Hospital, affiliated with Shanghai Jiao Tong University School of Medicine.

Data sharing statement

All relevant data are available from the corresponding author upon request.

References

[1] Eslam M, Newsome PN, Sarin SK, Anstee QM, Targher G, Romero-Gomez M, *et al*. A new definition for metabolic dysfunction-associated fatty liver disease: An international expert consensus statement. J Hepatol 2020; 73(1):202–209. doi:10.1016/j.jhep.2020.03.039, PMID:32278004.

[2] Fouad Y, Palmer M, Chen M, Regev A, Banerjee R, Myers R, *et al*. Redefinition of Fatty Liver Disease from NAFLD to MAFLD through the Lens of Drug Development and Regulatory Science. J Clin Transl Hepatol 2022;10(2):374–382. doi:10.14218/jcth.2021.00408, PMID:35528969.

[3] Younossi ZM, Koenig AB, Abdelatif D, Fazel Y, Henry L, Wymer M. Global epidemiology of nonalcoholic fatty liver disease-Meta-analytic assessment of prevalence, incidence, and outcomes. Hepatology 2016;64(1):73–84. doi:10.1002/hep.28431, PMID:26707365.

[4] Tilg H, Effenberger M. From NAFLD to MAFLD: when pathophysiology succeeds. Nat Rev Gastroenterol Hepatol 2020;17(7):387–388. doi:10.1038/s41575-020-0316-6, PMID:32461575.

[5] Jaako K, Waniek A, Parik K, Klimaviciusa L, Aonurm-Helm A, Noortoots A, *et al*. Prolyl endopeptidase is involved in the degradation of neural cell adhesion molecules in vitro. J Cell Sci 2016;129(20):3792–3802. doi:10.1242/jcs.181891, PMID:27566163.

[6] Svarcbahs R, Julku U, Kilpeläinen T, Kyyrö M, Jäntti M, Myöhänen TT. New tricks of prolyl oligopeptidase inhibitors - A common drug therapy for several neurodegenerative diseases. Biochem Pharmacol 2019;161:113–120. doi:10.1016/j.bcp.2019.01.013, PMID:30660495.

[7] Jiang DX, Zhang JB, Li MT, Lin SZ, Wang YQ, Chen YW, *et al*. Prolyl endopeptidase gene disruption attenuates high fat diet-induced nonalcoholic fatty liver disease in mice by improving hepatic steatosis and inflammation. Ann Transl Med 2020;8(5):218. doi:10.21037/atm.2020.01.14, PMID:32309365.

[8] Zhang J, Jiang D, Lin S, Cheng Y, Pan J, Ding W, *et al*. Prolyl endopeptidase disruption reduces hepatic inflammation and oxidative stress in methionine-choline-deficient diet-induced steatohepatitis. Life Sci 2021;270:119131. doi:10.1016/j.lfs.2021.119131, PMID:33516698.

[9] Weathington NM, van Houwelingen AH, Noerager BD, Jackson PL, Kraneveld AD, Galin FS, *et al*. A novel peptide CXCR ligand derived from extracellular matrix degradation during airway inflammation. Nat Med 2006;12(3):317–323. doi:10.1038/nm1361, PMID:16474398.

[10] Szul T, Bratcher PE, Fraser KB, Kong M, Tirouvanziam R, Ingersoll S, *et al*. Toll-Like Receptor 4 Engagement Mediates Prolyl Endopeptidase Release from Airway Epithelia via Exosomes. Am J Respir Cell Mol Biol 2016;54(3):359–369. doi:10.1165/rcmb.2015-0108OC, PMID:26222144.

[11] Kumar N, Nakagawa P, Janic B, Romero CA, Worou ME, Monu SR, *et al*. The anti-inflammatory peptide Ac-SDKP is released from thymosin-β4 by renal meprin-α and prolyl oligopeptidase. Am J Physiol Renal Physiol 2016;310(10):F1026–F1034. doi:10.1152/ajprenal.00562.2015, PMID:26962108.

[12] Chen YW, Liu BW, Zhang YJ, Chen YW, Dong GF, Ding XD, *et al*. Preservation of basal AcSDKP attenuates carbon tetrachloride-induced fibrosis in the rat liver. J Hepatol 2010;53(3):528–536. doi:10.1016/j.jhep.2010.03.027, PMID:20646773.

[13] Abdul Roda M, Sadik M, Gaggar A, Hardison MT, Jablonsky MJ, Braber S, *et al*. Targeting prolyl endopeptidase with valproic acid as a potential modulator of neutrophilic inflammation. PLoS One 2014;9(5):e97594. doi:10.1371/journal.pone.0097594, PMID:24835793.

[14] Shi Y, Zhou M, Yan J, Gong Z, Wu J, Chen Y, *et al*. N-Acetyl-Seryl-Aspartyl-Lysyl-Proline Mitigates Experimental Colitis Through Inhibition of Intestinal Mucosal Inflammatory Responses via MEK-ERK Signaling. Front Pharmacol 2020;11:593. doi:10.3389/fphar.2020.00593, PMID:32435194.

[15] Svarcbahs R, Julku UH, Myöhänen TT. Inhibition of Prolyl Oligopeptidase Restores Spontaneous Motor Behavior in the α-Synuclein Virus Vector-Based Parkinson's Disease Mouse Model by Decreasing α-Synuclein Oligomeric Species in Mouse Brain. J Neurosci 2016;36(49):12485–12497. doi:10.1523/JNEUROSCI.2309-16.2016, PMID:27927963.

[16] Savolainen MH, Richie CT, Harvey BK, Männistö PT, Maguire-Zeiss KA, Myöhänen TT. The beneficial effect of a prolyl oligopeptidase inhibitor, KYP-2047, on alpha-synuclein clearance and autophagy in A30P transgenic mouse. Neurobiol Dis 2014;68:1–15. doi:10.1016/j.nbd.2014.04.003, PMID:24746855.

[17] Jalkanen AJ, Leikas JV, Forsberg MM. KYP-2047 penetrates mouse brain and effectively inhibits mouse prolyl oligopeptidase. Basic Clin Pharmacol Toxicol 2014;114(6):460–463. doi:10.1111/bcpt.12184, PMID:24350801.

[18] Matthews DR, Hosker JP, Rudenski AS, Naylor BA, Treacher DF, Turner RC. Homeostasis model assessment: insulin resistance and beta-cell function from fasting plasma glucose and insulin concentrations in man. Diabetologia 1985;28(7):412–419. doi:10.1007/BF00280883, PMID:3899825.

[19] Zhang F, Hu Z, Li G, Huo S, Ma F, Cui A, *et al*. Hepatic CREBZF couples insulin to lipogenesis by inhibiting insig activity and contributes to hepatic steatosis in diet-induced insulin-resistant mice. Hepatology 2018;68(4):1361–1375. doi:10.1002/hep.29926, PMID:29637572.

[20] Zhou D, Pan Q, Xin FZ, Zhang RN, He CX, Chen GY, *et al*. Sodium butyrate attenuates high-fat diet-induced steatohepatitis in mice by improving gut microbiota and gastrointestinal barrier. World J Gastroenterol 2017;23(1):60–75. doi:10.3748/wjg.v23.i1.60, PMID:28104981.

[21] Li Y, Xu S, Mihaylova MM, Zheng B, Hou X, Jiang B, *et al*. AMPK phosphorylates and inhibits SREBP activity to attenuate hepatic steatosis and atherosclerosis in diet-induced insulin-resistant mice. Cell Metab 2011; 13(4):376–388. doi:10.1016/j.cmet.2011.03.009, PMID:21459323.

[22] Bataller R, Brenner DA. Liver fibrosis. J Clin Invest 2005;115(2):209–218. doi:10.1172/JCI24282, PMID:15690074.

[23] Sakaida I, Terai S, Yamamoto N, Aoyama K, Ishikawa T, Nishina H, *et al*. Transplantation of bone marrow cells reduces CCl4-induced liver fibrosis in mice. Hepatology 2004;40(6):1304–1311. doi:10.1002/hep.20452, PMID:15565662.

[24] Goodman ZD. Grading and staging systems for inflammation and fibrosis in chronic liver diseases. J Hepatol 2007;47(4):598–607. doi:10.1016/j.jhep.2007.07.006, PMID:17692984.

[25] Kleiner DE, Brunt EM, Van Natta M, Behling C, Contos MJ, Cummings OW, *et al*. Design and validation of a histological scoring system for nonalcoholic fatty liver disease. Hepatology 2005;41(6):1313–1321. doi:10.1002/hep.20701, PMID:15915461.

[26] Bjørkøy G, Lamark T, Brech A, Outzen H, Perander M, Overvatn A, *et al*. p62/SQSTM1 forms protein aggregates degraded by autophagy and has a protective effect on huntingtin-induced cell death. J Cell Biol 2005;171(4):603–614. doi:10.1083/jcb.200507002, PMID:16286508.

[27] Chao X, Ni HM, Ding WX. Insufficient autophagy: a novel autophagic flux scenario uncovered by impaired liver TFEB-mediated lysosomal biogenesis from chronic alcohol-drinking mice. Autophagy 2018;14(9):1646–1648. doi:10.1080/15548627.2018.1489170, PMID:29969942.

[28] Penttinen A, Tenorio-Laranga J, Siikanen A, Morawski M, Rossner S, García-Horsman JA. Prolyl oligopeptidase: a rising star on the stage of neuroinflammation research. CNS Neurol Disord Drug Targets 2011;10(3):340–348. doi:10.2174/187152711794653742, PMID:21222623.

[29] Natunen TA, Gynther M, Rostalski H, Jaako K, Jalkanen AJ. Extracellular prolyl oligopeptidase derived from activated microglia is a potential neuroprotection target. Basic Clin Pharmacol Toxicol 2019;124(1):40–49. doi:10.1111/bcpt.13094, PMID:29998529.

[30] Zhou D, Li BH, Wang J, Ding YN, Dong Y, Chen YW, *et al*. Prolyl Oligopeptidase Inhibition Attenuates Steatosis in the L02 Human Liver Cell Line. PLoS One 2016;11(10):e0165224. doi:10.1371/journal.pone.0165224, PMID:27760195.

[31] Myöhänen TT, Venäläinen JI, García-Horsman JA, Piltonen M, Männistö PT. Distribution of prolyl oligopeptidase in the mouse whole-body sections and peripheral tissues. Histochem Cell Biol 2008;130(5):993–1003. doi:10.1007/s00418-008-0468-x, PMID:18618130.

[32] Lazo M, Solga SF, Horska A, Bonekamp S, Diehl AM, Brancati FL, *et al*. Effect of a 12-month intensive lifestyle intervention on hepatic steatosis in adults with type 2 diabetes. Diabetes Care 2010;33(10):2156–2163. doi:10.2337/dc10-0856, PMID:20664019.

[33] Höfling C, Kulesskaya N, Jaako K, Peltonen I, Männistö PT, Nurmi A, *et al*. Deficiency of prolyl oligopeptidase in mice disturbs synaptic plasticity and reduces anxiety-like behaviour, body weight, and brain volume. Eur Neuropsychopharmacol 2016;26(6):1048–1061. doi:10.1016/j.euroneuro.2016.02.015, PMID:26996375.

[34] Sánchez-Garrido MA, Habegger KM, Clemmensen C, Holleman C, Müller TD, Perez-Tilve D, *et al*. Fibroblast activation protein (FAP) as a novel metabolic target. Mol Metab 2016;5(10):1015–1024. doi:10.1016/j.molmet.2016.07.003, PMID:27689014.

[35] Schuster S, Cabrera D, Arrese M, Feldstein AE. Triggering and resolution of inflammation in NASH. Nat Rev Gastroenterol Hepatol 2018;15(6):349–364. doi:10.1038/s41575-018-0009-6, PMID:29740166.

[36] Tenorio-Laranga J, Montoliu C, Urios A, Hernandez-Rabaza V, Ahabrach H, García-Horsman JA, *et al*. The expression levels of prolyl oligopeptidase responds not only to neuroinflammation but also to systemic inflammation upon liver failure in rat models and cirrhotic patients. J Neuroinflammation 2015;12:183. doi:10.1186/s12974-015-0404-7, PMID:26420028.

[37] Maes M, Goossens F, Scharpé S, Calabrese J, Desnyder R, Meltzer HY. Alterations in plasma prolyl endopeptidase activity in depression, mania, and schizophrenia: effects of antidepressants, mood stabilizers, and antipsychotic drugs. Psychiatry Res 1995;58(3):217–225. doi:10.1016/0165-1781(95)02698-v, PMID:8570777.

[38] Kamori M, Hagihara M, Nagatsu T, Iwata H, Miura T. Activities of dipeptidyl peptidase II, dipeptidyl peptidase IV, prolyl endopeptidase, and collagenase-like peptidase in synovial membrane from patients with rheumatoid arthritis and osteoarthritis. Biochem Med Metab Biol 1991;45(2):154–160. doi:10.1016/0885-4505(91)90016-e, PMID:1679339.

[39] Gaggar A, Jackson PL, Noerager BD, O'Reilly PJ, McQuaid DB, Rowe SM, *et al*. A novel proteolytic cascade generates an extracellular matrix-derived chemoattractant in chronic neutrophilic inflammation. J Immunol 2008;180(8):5662–5669. doi:10.4049/jimmunol.180.8.5662, PMID:183

90751.
[40] Kumar S, Duan Q, Wu R, Harris EN, Su Q. Pathophysiological communication between hepatocytes and non-parenchymal cells in liver injury from NAFLD to liver fibrosis. Adv Drug Deliv Rev 2021;176:113869. doi: 10.1016/j.addr.2021.113869, PMID:34280515.
[41] Li L, Xu M, He C, Wang H, Hu Q. Polystyrene nanoplastics potentiate the development of hepatic fibrosis in high fat diet fed mice. Environ Toxicol 2022;37(2):362–372. doi:10.1002/tox.23404, PMID:34755918.
[42] Helsley RN, Varadharajan V, Brown AL, Gromovsky AD, Schugar RC, Ramachandiran I, *et al*. Obesity-linked suppression of membrane-bound O-acyltransferase 7 (MBOAT7) drives non-alcoholic fatty liver disease. Elife 2019;8:e49882. doi:10.7554/eLife.49882, PMID:31621579.
[43] Svarcbahs R, Julku UH, Norrbacka S, Myöhänen TT. Removal of prolyl oligopeptidase reduces alpha-synuclein toxicity in cells and in vivo. Sci Rep 2018;8(1):1552. doi:10.1038/s41598-018-19823-y, PMID:29367610.
[44] Svarcbahs R, Jäntti M, Kilpeläinen T, Julku UH, Urvas L, Kivioja S, *et al*. Prolyl oligopeptidase inhibition activates autophagy via protein phosphatase 2A. Pharmacol Res 2020;151:104558. doi:10.1016/j.phrs.2019.104558, PMID:31759088.
[45] Hellinen L, Koskela A, Vattulainen E, Liukkonen M, Wegler C, Treyer A, *et al*. Inhibition of prolyl oligopeptidase: A promising pathway to prevent the progression of age-related macular degeneration. Biomed Pharmacother 2022;146:112501. doi:10.1016/j.biopha.2021.112501, PMID:34891119.
[46] Yang RX, Pan Q, Liu XL, Zhou D, Xin FZ, Zhao ZH, *et al*. Therapeutic effect and autophagy regulation of myriocin in nonalcoholic steatohepatitis. Lipids Health Dis 2019;18(1):179. doi:10.1186/s12944-019-1118-0, PMID:31639005.
[47] Wu X, Poulsen KL, Sanz-Garcia C, Huang E, McMullen MR, Roychowdhury S, *et al*. MLKL-dependent signaling regulates autophagic flux in a murine model of non-alcohol-associated fatty liver and steatohepatitis. J Hepatol 2020;73(3):616–627. doi:10.1016/j.jhep.2020.03.023, PMID:32220583.
[48] Wang Y, Zhao H, Li X, Li N, Wang Q, Liu Y, *et al*. Tangshen Formula Alleviates Hepatic Steatosis by Inducing Autophagy Through the AMPK/SIRT1 Pathway. Front Physiol 2019;10:494. doi:10.3389/fphys.2019.00494, PMID:31105592.
[49] Qian H, Chao X, Williams J, Fulte S, Li T, Yang L, *et al*. Autophagy in liver diseases: A review. Mol Aspects Med 2021;82:100973. doi:10.1016/j.mam.2021.100973, PMID:34120768.